Dyslipidemia at the crossroad of the skin barrier and the arterial wall

Martins Cardoso, R.

Chapter 2

Hypercholesterolemia in young adult *APOE*$^{-/-}$ mice alters epidermal lipid composition and impairs barrier function

Biochimica et Biophysica Acta Molecular and Cell Biology of Lipids 1864(7): 976-984 (2019).

Renata Martins Cardoso[1], Eline Creemers[1], Samira Absalah[1], Gert S. Gooris[1], Menno Hoekstra[1], Miranda Van Eck[1*], Joke A. Bouwstra[1*]

[1]Division of BioTherapeutics, Leiden Academic Centre for Drug Research, Leiden University, Leiden, The Netherlands

*Both authors contributed equally

ABSTRACT

Long-term exposure to hypercholesterolemia induces the development of skin xanthoma's characterized by the accumulation of lipid-laden foam cells in humans and in mice. Early skin changes in response to hypercholesterolemia are however unknown. In this study, we investigated the skin lipid composition and associated barrier function in young adult low-density lipoprotein receptor knockout (*LDLR*$^{-/-}$) and apolipoprotein E knockout (*APOE*$^{-/-}$) mice, two commonly used hypercholesterolemic mouse models characterized by the accumulation of apolipoprotein B containing lipoproteins. No effects were observed on cholesterol content in the epidermis in *LDLR*$^{-/-}$ mice or in the more extremely hypercholesterolemic *APOE*$^{-/-}$ mice. Interestingly, the free fatty acids in the *APOE*$^{-/-}$ epidermis shifted towards shorter and unsaturated chains. Genes involved in the synthesis of cholesterol and fatty acids were downregulated in *APOE*$^{-/-}$ skin suggesting a compensation for the higher influx of plasma lipids, most probably as cholesteryl esters. Importantly, *in vivo* transepidermal water loss and permeability studies with murine lipid model membranes revealed that the lipid composition of the *APOE*$^{-/-}$ skin resulted in a reduced skin barrier function. In conclusion, severe hypercholesterolemia associated with increased apolipoprotein B containing lipoproteins affects the epidermal lipid composition and its protective barrier.

Keywords: *skin barrier lipids; apolipoprotein E knockout; low-density lipoprotein receptor knockout; free fatty acids; cholesteryl esters; LC/MS.*

1. INTRODUCTION

Patients suffering from familial hypercholesterolemia often present mutations in the low-density lipoprotein receptor (LDLR) or other proteins (*e.g.* apolipoprotein E - apoE) that result in increased circulating levels of low-density lipoprotein and a higher risk of developing cardiovascular diseases[1–3]. Interestingly, these patients are also reported to develop skin xanthoma's filled with cholesterol-laden macrophages[4,5]. Lipid-lowering therapy with statins is the main choice of treatment for hypercholesterolemic patients[1,4]. However, in some cases statin treatment is not sufficient to reverse the skin phenotypes[3,5].

Hypercholesterolemia has been extensively studied using LDLR knockout (*LDLR*$^{-/-}$) and APOE knockout (*APOE*$^{-/-}$) mice. Both LDLR and apoE play an essential role in the clearance of apolipoprotein B and apoE containing lipoproteins from the circulation by the liver[6,7]. In the absence of a functional LDLR, the clearance of apolipoprotein B and apoE containing lipoproteins is impaired leading to accumulation of these particles in the plasma. However, as apoE containing lipoproteins are also cleared by LDLR-related protein 1 (LRP1), *LDLR*$^{-/-}$ mice develop a mild hypercholesterolemia on a regular chow diet or severe hypercholesterolemia when fed a high fat/high cholesterol diet[6,7]. *APOE*$^{-/-}$ mice, on the other hand, develop a more severe hypercholesterolemic phenotype on chow diet as the lipoprotein clearance by both the LDLR and LRP1 are impaired[6,7].

Similar to hypercholesterolemic patients, xanthoma's have also been described in the skin of *LDLR*$^{-/-}$ mice and *APOE*$^{-/-}$ mice. On a low-fat diet the morphology of the skin of young adult *LDLR*$^{-/-}$ and *APOE*$^{-/-}$ mice is comparable to the wild-type (WT) control of similar age with no signs of inflammation or lipid deposits[8–11]. However, on a high fat/high cholesterol diet both *LDLR*$^{-/-}$ mice and *APOE*$^{-/-}$mice showed accumulation of fat droplets and inflammatory infiltrates in their skin[10–12]. Furthermore, aging of *APOE*$^{-/-}$ mice fed low-fat diet exhibited skin phenotypes characterized by skin thinning, hair follicle loss and premature greying of the hair accompanied by impaired hair regeneration, which appeared earlier than reported for WT controls[13,14]. Also, these age-related skin changes can be accelerated when *APOE*$^{-/-}$ mice received high fat/high cholesterol diet[13].

The skin naturally functions as a barrier protecting the body from excessive water and electrolyte loss and permeation of harmful agents and pathogens. This protective function is mostly performed by corneocytes and an extracellular lipid domain present in the outermost layer of the epidermis, the stratum corneum (SC)[15]. The SC lipid domain mainly comprises cholesterol, ceramides (CERs) and free fatty acids (FFAs), which

are primarily synthesized by keratinocytes during their differentiation process[16]. In addition to local lipid synthesis, keratinocytes express receptors involved in the uptake of lipids from plasma, (*e.g.* LDLR, scavenger receptor class B member I and cluster of differentiation 36) via which plasma lipids likely enter the skin and can be detected in the epidermis[17–19].

Despite the crucial role of lipids in the skin barrier, the early consequences of an impaired metabolism of apolipoprotein B and apoE containing lipoproteins to the skin lipid composition and barrier function are unknown. In this study we compared young adult *LDLR*$^{-/-}$ mice and *APOE*$^{-/-}$ mice with WT controls of the same age and genetic background to specifically analyze the effects of hypercholesterolemia on skin morphology, lipid composition and organization, and barrier functionality prior to the development of inflammatory phenotypes as described for high fat/high cholesterol diets and aging.

2. MATERIALS AND METHODS

2.1 Chemicals

Manufacture's details regarding the chemicals used in these studies are available in the online supplementary information.

2.2 Animals

16-18 weeks old female WT, homozygous *LDLR*$^{-/-}$ mice and homozygous *APOE*$^{-/-}$ mice (obtained from The Jackson laboratory and bred at the Gorlaeus laboratories) all on a C57BL/6 background were kept under standard laboratory conditions (20^{o}C and light cycle of 12h light/12h dark) with water and standard low fat chow diet ad libitum (Rat and Mouse No.3 breeding diet, Special Diets Services, United Kingdom) and not fasted prior sacrifice. All experiments were performed in accordance with National guidelines and approved by the Ethics Committee for Animals Experiments of Leiden University. The mice were anesthetized for retro-orbital bleeding (70 mg/kg body weight xylazine, 1.8 mg/kg body weight atropine, 350 mg/kg body weight ketamine) and shaving of the back skin followed by perfusion with phosphate buffered saline (PBS, pH 7.4 - 8.13 g/L NaCl, 2.87 g/L Na_2HPO_4, 0.2 g/L KH_2PO_4, 0.19 g/L KCl in milliQ water) at room temperature.

2.3 Plasma lipid analysis

Enzymatic colorimetric assays were used to measure non-fasted plasma levels of

cholesterol and triglycerides (Roche Diagnostics, Almere, Netherlands)[20]. All assays were performed according to manufacturer's instructions.

2.4 Skin morphology staining

Paraffin embedded skin sections (4-5 µm) were deparaffinized, rehydrated and stained with hematoxylin and eosin according to manufacturer's instructions or with toluidine blue. In short, toluidine blue stock solution (1% w/v in 70 % ethanol) was diluted 10 times in NaCl solution (1% w/v in demi-water). Skin sections were deparaffinized, rehydrated, stained for 2 min with toluidine blue working solution, and rinsed with demi-water. For both stainings slides were mounted in Entellan® and the sections were imaged with a Zeiss Axioplan 2 light microscope (Zeiss, Best, The Netherlands) and BH-2 polarized microscope (Olympus, Leiderdorp, The Netherlands).

2.5 Liquid chromatography-mass spectrometry (LC/MS)

After removing the hypodermis, skin samples were placed overnight (4°C) on a paper filter soaked with 0.3 % w/v trypsin solution in PBS (pH 7.4). Next day, the samples were incubated at for 1 hour at 37°C to isolate the epidermis. Next, the epidermis was rinsed once in 0.1% w/v trypsin inhibitor in PBS and twice in demi-water. The samples dried at room temperature and were stored under argon atmosphere for lipids extraction and FTIR measurements. Epidermal lipids were extracted as described by Boiten *et al.* (2016)[21] and the extracts were stored in chloroform:methanol (2:1; v/v) at 4°C under argon atmosphere for cholesterol, CER and FFA analyses.

Cholesterol and CER analysis

Lipid extracts were dried and reconstituted in heptane:chloroform:methanol (95:2.5:2.5; v/v/v) to a lipid concentration of 0.3 mg/mL. 5 µl of reconstituted lipid extracts were injected in an Acquity UPLC H-class system (Waters, Milford, MA, USA) connected to a triple-quadrupole XEVO TQ-S mass spectrometer (Waters, Milford, MA, USA). Separation occurred in a normal phase column (PVA-Sil column: 5 µm particle size, 100x2.1 mm i.d., YMC, Kyoto, Japan) at flow rate of 0.8 ml/min with a gradient solvent shift from 98% heptane and 2% heptane:isopropanol:ethanol (50:25:25; v/v/v) to 50% heptane and 50% heptane:isopropanol:ethanol (50:25:25; v/v/v) in 11 minutes (Supplementary Table S1). The mass spectrometer was coupled to atmospheric pressure chemical ionization chamber set to positive ion mode and the detector measured in full scans from 350-1200 amu. Deuterated CER[NS] (C24deuterated; C18protonated) was added to all samples as internal standard prior to injection into UPLC/MS. Software

Waters MassLynx 4.1 was used to determine the area under the curve (AUC) followed by internal standard correction for both cholesterol and CER analysis. Cholesterol AUC was further corrected for the response based on a calibration curve of cholesterol and the data was plotted as absolute amount of cholesterol (µg) per epidermis weight (mg). CER composition was provided as AUC corrected for the internal standard and was plotted as relative percentage of ceramide subclasses. CER subclasses were named as described previously[22] based on different acyl chains (non-hydroxy fatty acid [N]; α-hydroxy fatty acid [A]; esterified ω-hydroxy fatty acid [EO]) and on the sphingoid base (dihydrosphingosine, [dS]; sphingosine [S]; phytosphingosine [P]) (Supplementary Fig. S1).

FFA analysis

Lipid extracts were dried and reconstituted in isopropanol to a lipid concentration of 0.75 mg/mL. 2 µl of reconstituted lipid extracts were injected in the same UPLC-mass spectrometry system described in subsection "Cholesterol and CERs analysis". Deuterated FFA C18 and FFA C24 were added to all samples as internal standard. FFA separation in the UPLC H-class system was done with Purospher Star LiChroCART reverse phase column (3 µm particle size, 55x2 mm i.d., 55x2 mm, Merck, Darmstadt, Germany) with a solvent shift from 100% acetonitrile/milliQ/chloroform/acetic acid (90:10:2:0.005; v/v/v/v) to 100% methanol/heptane/chloroform/acetic acid (90:10:2:0.005; v/v/v/v) in 2.5 minutes at a flow rate of 0.5 mL/min (Supplementary Table S2). The XEVO TQ-S mass spectrometer was connected to an atmospheric pressure chemical ionization chamber (probe temperature: 425°C, discharge current 3 µA.) set to negative mode and detector measured in full scan from 200-550 amu. Data analysis was performed by Waters MassLynx 4.1 and the area under the curve (AUC) was corrected by the internal standard FFA C24 and corrected for the response based on calibration curves of FFA C16-C30. Data was plotted as absolute amounts and relative percentage to the total amount of FFA detected. FFA C16:0 and C18:0 were not included due to manufacturer's contamination of the chloroform extracting solvent with these FAs. Unsaturated FFA C16-C18 were plotted separately as they also are important components of sebum lipids.

2.6 Quantitative real-time PCR (q-PCR)

Total RNA from skin samples without hypodermis were isolated by guanidinium thiocyanate method[23]. cDNA was synthesized from 1 µg RNA with M-MuLV reverse transcriptase. Quantitative gene analysis was done with 7500 Fast real-time PCR system (Applied Biosystems, Foster City, CA, USA) using SYBR Green Technology as detection

method. Ribosomal protein, large, P0 (*RPL0*), cytochrome c-1 (*CYC1*) and ribosomal protein S20 (*RPS20*) were used as housekeeping genes. Relative gene expression was calculated by deducting the average threshold cycle (Ct) of the housekeeping genes from the Ct of the target gene. The difference was then raised to 2 to the power and the data was plotted as relative fold change compared to the WT control group. Primer sequences of the analyzed genes are available in Supplementary Table S3.

2.7 Fourier transform infrared spectroscopy (FTIR)

FTIR measurements were performed with Varian 670-IR spectrometer (Agilent Technologies, Inc., Santa Clara, CA) equipped with a broad-band mercury cadmium telluride detector. Hydrated epidermis (24 hours in 27% NaBr in deuterated water, D_2O) was mounted between 2 silver bromide windows for collection of FTIR spectra (600-4000 cm^{-1}) with resolution of 1 cm^{-1} in a temperature range from 0-90°C (0.5°C/min). Spectra were analyzed and deconvoluted (half width of 4cm-1; enhancement factor of 1.7) with Resolutions Pro 4.1 (Varian Inc.) software. CH_2 rocking vibrations were used to determine the orthorhombicity of the samples and the transition temperature from orthorhombic to hexagonal phases. The area ratio (peak area at 730 cm^{-1}/ peak area at 719 cm^{-1}) was calculated by curve fitting the FTIR spectra at 32°C in the range of CH_2 rocking vibrations (710-740 cm^{-1}). In this range, two peaks were fitted using a Lorentzian peak function. The transition temperature between the orthorhombic and hexagonal phases was determined by the disappearance of the peak at the 730 cm^{-1}. CH_2 asymmetrical stretching vibrations (2840-2860 cm^{-1}) were monitored to assess the conformational ordering of the lipid chains.

2.8 Transepidermal water loss (TEWL)

The barrier function of the skin of WT and *APOE*$^{-/-}$ mice was examined by measuring the transepidermal water loss (TEWL). The measurements were performed under controlled ambient temperature (22°C) and humidity (49.5%). The mice were anesthetized as described in section 2.2, their back skin was shaved and the closed-chamber of the evaporimeter (Aqua Flux AF200, Biox Systems Ltd, London, UK) was placed on their back skin in upright position perpendicular to the skin surface. Transepidermal water loss was measured for 90 seconds.

2.9 Preparation of murine lipid model membranes (mLMM)

Synthetic mLMMs were prepared in a composition representing the epidermal lipid composition of the WT and the *APOE*$^{-/-}$ mice. The membranes contained an equimolar

ratio of synthetic CER, FFA and cholesterol. All mLMM CER mixture were prepared with CER NdS C24, CER NS C24, CER NP C24, CER AS C24, CER EOS C30 lineolate (40.5: 36:5:14.5:4, respective molar ratios). FFA mixtures were composed of FFA C16:0, C18:0, C20:0, C20:1, C22:0, C22:1, C24:0, C26:0 in a molar ratio of 3.5:1.5:2.0: 10.0:4.5:3.5:30.0:45.0, representative of WT epidermis or 4.5:0.5:12.5:31.5:7.5:6.0:22 .0:15.50, mimicking lipid composition of *APOE*$^{-/-}$ epidermis. mLMM were prepared as described previously[24]. In short, lipid mixtures (5 mg/mL in a 100 µL Hamilton syringe, Bonaduz, Switzerland) in hexane:ethanol (2:1, v/v) were sprayed onto a polycarbonate membrane (0.05 µm pore size, 25 mm i.d., Whatmann, Kent, UK) using a Camag Linomat IV with an extended y-axis arm (Muttenz, Switzerland). Mixtures were sprayed at a 5 µL/min flow under a gentle nitrogen flow to form a homogenous square (8x8 mm). Afterwards, the membranes were equilibrated at 85°C for 10 minutes, cooled down to room temperature and stored in the dark under argon atmosphere for characterization by X-ray diffraction studies and permeability studies.

2.10 X-ray diffraction studies on mLMM

The lamellar and lateral organizations of the mLMM were assessed by X-ray diffraction measurements performed at the station BM26B of the European Synchrotron Radiation facility (ESRF, Grenoble, France). For measurements, mLMM were hydrated for 24 hours (27% NaBr in demiwater) prior mounting in parallel to the primary beam in a sample holder with temperature controlled (25°C). Data were collected with a Pilatus 1M detector (1043 × 981 pixels at 172 x 172 µm spatial resolution) for small angle x-ray diffraction (SAXD) and with a Pilatus 300K (1475 × 195 pixels at 172 x 172 µm spatial resolution) for wide angle X-ray diffraction (WAXD). SAXD detector was calibrated using silver behenate (d = 5.838 nm) and the WAXD detector was calibrated using the two strongest reflections of high density polyethylene (HDPE, d = 0.416 and 0.378 nm). Cholesterol was also used as an internal standard as it is often a component of our synthetic lipid membranes. The X-ray wavelength was 0.1034 nm and the sample-to-detector distances were 1980 mm for Pilatus 1M detector and 3110 mm to the Pilatus 300K detector. Static measurements patterns were collected for 60 seconds and the scattering intensity I (in arbitrary units) was measured and calculated as a function of the scattering vector q (in reciprocal nm). Vector q was defined as $q = (4\pi \sin \theta)/\lambda)$ with θ representing the scattering angle and λ the wavelength. Using the positions of a sequence of equidistant peaks (q_n), the periodicity (d-spacing) of a lamellar phase was calculated ($q_n = 2n\pi/d$, n representing the order number of the diffraction peak). Peaks were integrated in a 40° angle perpendicular to the sample in the X-ray beam.

2.11 Permeability of mLMM to E-PABA

The barrier function of the murine epidermis lipids was investigated by the permeability of the mLMM to the model drug ethyl para-aminobenzoic acid (E-PABA; MW: 165.189 g/mol). For the permeation studies flow through Permegear inline diffusion cells (Bethlehem PA, USA) were used. mLMM were mounted into the diffusion cells (0.282 cm^2 diffusion area) and hydrated for at least 1 hour in the PBS acceptor phase (pH 7.4, filtered and degassed). The donor phase was a saturated and filtered E-PABA solution (concentration 0.65 mg/mL) in sodium acetate buffer (pH 5.0; 0.1 M acetic acid, 0.1 M sodium acetate, 1:2.5; v/v). To avoid evaporation from the donor phase adhesive tape was used to close the donor compartment. The acceptor phase was under constant stirring at 50 rpm perfused and perfused at a flow rate of 2-2.5 mL/min. The acceptor phase was sampled every hour for 10.5 hours (Isco Retriever IV; Teledyne Isco, Lincoln NE, USA). The amount of E-PABA in each sampled fraction was determined by UPLC-UV (Waters, Etten-Leur, The Netherlands) with a reversed phase C18 column (Alltima, C-18, 1.7 µm i.d., 2.1 x 50 mm, Waters, Ireland) at 40°C and an UV detector with excitation wavelength at 286 nm. The mobile phase consisted of acetonitrile with 0.1% trifluoroacetic acid :milliQ (40:60; v/v) at flow rate of 0.5mL/min. A calibration curve of E-PABA in ethanol was also measured. The software TargetLynx was used to process the data and calculate the flux of E-PABA.

2.12 Statistical analysis

Statistical analysis was performed using GraphPad Prism 7 (GraphPad Software Inc., CA, USA). Statistically significant differences between two groups were determined by two-tailed, unpaired Student's t-tests while differences among three groups were determined using One-way or Two-way ANOVAs with Holm-Šídák post-hoc test. Data is presented as mean ± SD and *p* values below 0.05 were considered significant.

3. RESULTS

3.1 Deficiency of *LDLR* or *APOE* results in (mild) hypercholesterolemia in chow-fed young adult mice but the skin morphology is preserved.

Non-fasted plasma lipid levels were determined by colorimetric enzymatic assays (Fig. 1a). On chow diet, *LDLR*$^{-/-}$ mice developed a mild hypercholesterolemia with increased plasma levels of free cholesterol (0.97±0.15 µg/µl plasma) and cholesteryl esters (CE) (2.05±0.54 µg/µl plasma) compared to WT controls (free cholesterol 0.36±0.05 µg/µl plasma and CE 0.97±0.15 µg/µl plasma). *APOE*$^{-/-}$mice on the same diet showed severe

hypercholesterolemia marked by 6-fold higher free cholesterol (2.3±0.49 µg/µl plasma) and 5-fold higher CE (4.59±1.03 µg/µl plasma). Plasma triglycerides were comparable among WT (1.02±0.15 µg/µl plasma), *LDLR*$^{-/-}$ (1.10±0.25 µg/µl plasma), and *APOE*$^{-/-}$ (1.13±0.16 µg/µl plasma) mice.

Subsequently, we assessed the impact of hypercholesterolemia on the skin morphology by hematoxylin and eosin and toluidine blue stainings (Fig. 1b). Hypercholesterolemic *LDLR*$^{-/-}$ and *APOE*$^{-/-}$ mice displayed similar skin morphology as the normolipidemic WT controls with a consistent number of epidermal layers (no hyperproliferation) and thin SC. In the dermis no striking morphological alterations or signs of inflammation were observed. Polarized light microscopy on skin sections did not show the presence of cholesterol crystals in the dermis.

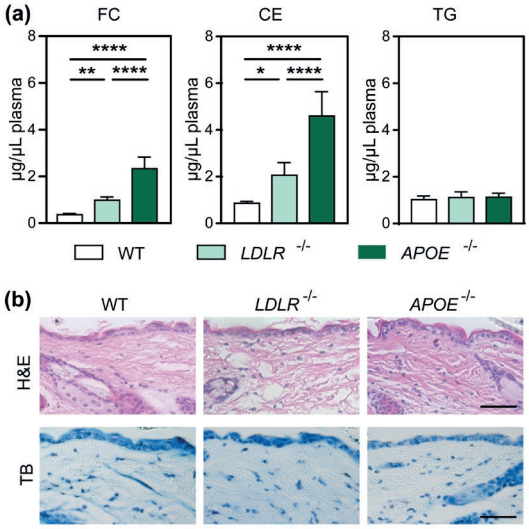

Figure 1. Chow-fed young-adult *APOE*$^{-/-}$ mice develop severe hypercholesterolemia but their skin shows no morphological changes or signs of inflammation compared to the chow-fed *LDLR*$^{-/-}$ mice and WT controls. (a) Plasma levels of free cholesterol (FC), cholesteryl esters (CE), and triglycerides (TG) were measured with enzymatic colorimetric assays. Animals were not fasted prior sacrifice (n= 4-6 animals/group). (b) Hematoxylin and eosin (H&E) and toluidine blue (TB) stainings of sections imaged with brightfield microscope (scale bar= 50 µm; representative images of n=3 animals/group; *p<0.05, **p <0.01, ****p<0.0001).

3.2 Increased amounts of shorter and unsaturated FFA species are present in the epidermis of *APOE*$^{-/-}$ but not in *LDLR*$^{-/-}$ mice

To examine whether the skin barrier was affected the three main SC lipid classes were analyzed by liquid-chromatography mass spectrometry (LC/MS). The amount of cholesterol did not differ among groups (Fig. 2a). Seven CER subclasses (detailed nomenclature as described by Motta *et al.* (1993) in Supplementary Fig. S1) were identified in the murine skin: CER NdS, CER NS, CER NP, CER AdS, CER AS, CER [EO], the latter representing CER EOdS and CER EOS (Fig. 2b). Abundance of CER NdS was significantly higher in *LDLR*$^{-/-}$ and *APOE*$^{-/-}$ epidermis (45% compared to 40% for WT controls) while the CER AS was lower in these mice (9% compared to 16% for WT controls). The average total CER chain length was 43-44 carbon atoms regardless the genetic background of the mice (Fig. 2c) and the ratio CER [EO]/CER [non-EO] both did not change (Supplementary Fig. S2a). CER NP and CER AdS could not be separated, thus these CERs are reported together representing about 5% of the total CERs.

Next, FFAs with chain length ranging from 20-30 carbon atoms were analyzed (Fig. 2d and Supplementary Fig. S2b). The epidermal FFA profile of the severely hypercholesterolemic *APOE*$^{-/-}$ mice strongly differed from that observed for the normolipidemic WT control and mild hypercholesterolemic *LDLR*$^{-/-}$ mice (Fig 2d-g). The *APOE*$^{-/-}$ epidermis contained 3 times the amount of FFA (Fig. 2e) with a 5-fold increase in the relative abundance of unsaturated FFA compared to WT and *LDLR*$^{-/-}$ epidermis, particularly the levels of FFA C20:1 were increased (Fig. 2d/f). In addition, *APOE*$^{-/-}$ epidermis showed a shift towards shorter FFA chains with on average 23 carbon atoms whilst in WT and *LDLR*$^{-/-}$ epidermis this average was around 25 carbon atoms (Fig. 2g). Over 50% of the FFA species in the *APOE*$^{-/-}$ epidermis contained less than 24 carbon atoms whilst for WT and *LDLR*$^{-/-}$ epidermis this value was around 20% (Supplementary Fig. S2c). In summary, in the *APOE*$^{-/-}$ epidermis FFA C20:1 was the most abundant FFA (25%) followed by FFA C24:0 (21%) and FFA C26:0 (16%) while for WT and *LDLR*$^{-/-}$ the most abundant species were FFA C24:0 and C26:0 representing nearly 28% and 40%, respectively. Additionally, the composition of unsaturated FFAs (C16-C18) was also altered in the *APOE*$^{-/-}$ epidermis with marked increase in the amounts of C16:1 (16-fold), C18:1 (18-fold) and C18:2 (8-fold) compared to the WT control (Supplementary Fig. S2d).

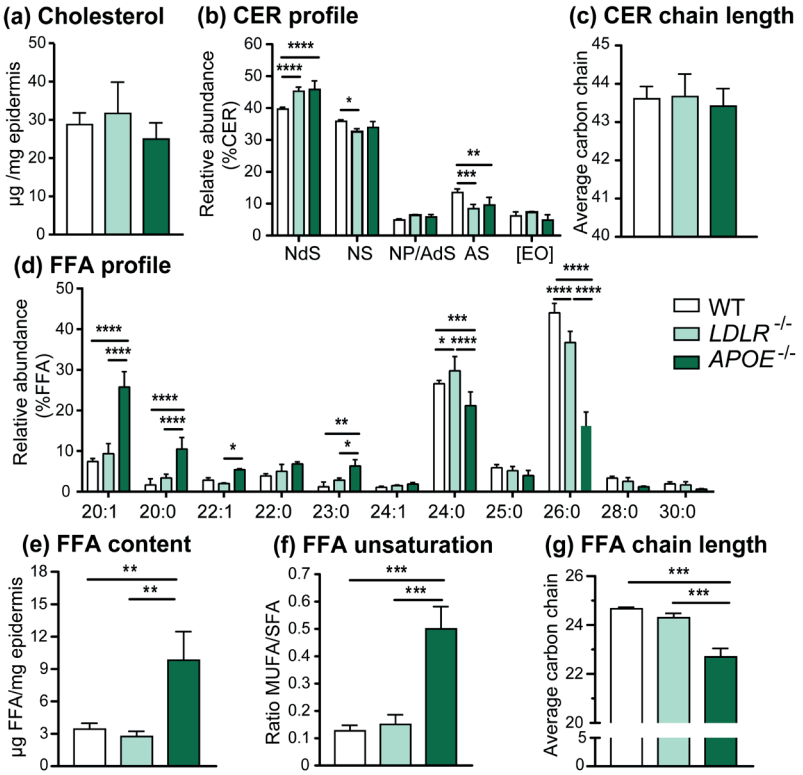

Figure 2. *APOE*$^{-/-}$ mice shows remarkably altered epidermal FFA profile compared to WT and *LDLR*$^{-/-}$ mice, while cholesterol and ceramides are not/minimally affected. LC/MS analysis of the three main classes of SC lipids: (a) cholesterol, (b-c) CERs, (d-g) FFAs. CER data plotted as a percentage of the total peak area after correction by internal standard. Nomenclature of ceramides subclasses based on different acyl chains (non-hydroxy fatty acid [N]; α-hydroxy fatty acid [A]; esterified ω-hydroxy fatty acid [EO]) and on the sphingoid base (dihydrosphingosine, [dS]; sphingosine [S]; phytosphingosine [P]). CER[EO] represents CER EOS and CER EOdS (n=3/group; *p<0.05; **p<0.01; ***p<0.001; ****p<0.0001).

3.3 *APOE*$^{-/-}$ mice downregulate cholesterol and FFA synthesis genes in the skin

The epidermal FFA composition of the *APOE*$^{-/-}$ mice greatly differed from that of the WT controls. Therefore, the expression of genes involved in lipid synthesis and uptake from circulation was assessed by quantitative real-time polymerase chain reaction (q-PCR) and compared to the WT controls to gain insight in the mechanisms underlying the changes in epidermal barrier lipids of *APOE*$^{-/-}$mice (Fig. 3). Expression of cholesterol synthesis and uptake genes was reduced in the skin of *APOE*$^{-/-}$ mice as

evidenced by the strong downregulation of *HMGCR* and *LDLR* (Fig. 3a). Expression of ATP-binding cassette genes (*ABCA1*, *ABCA12*, *ABCG1*) showed no differences between groups (Supplementary Fig. S3a). The expression of *CERS3* was not changed while *GBA* expression involved in the metabolism of glycolipids in the skin was downregulated in *APOE*$^{-/-}$ mice (Fig. 3b). No changes in expression were observed for CER degradation genes (Supplementary Fig. S3b). Genes involved in FFA synthesis (*ACACA*) and FFA elongation (*ELOVL1*) were remarkably reduced in the *APOE*$^{-/-}$ mice but no changes were observed between groups regarding FFA chain desaturation (*SCD1*) (Fig. 3c). Expression of other elongases (*ELOVL4, ELOVL6, ELOVL7*) and fatty acid transporters (*FABP5, CD36*) was not changed (Supplementary Fig. S3c-d). Furthermore, we evaluated whether the adapted lipid metabolism in the *APOE*$^{-/-}$ skin could affect keratinocyte proliferation and differentiation markers. However, mRNA levels of the proliferation marker *Ki-67*, early differentiation marker *K10*, late differentiation markers *IVL* and *FLG* did not differ in *APOE*$^{-/-}$ skin compared to WT skin (Supplementary Fig. S3e). Additionally, the q-PCR data did not reveal upregulation of pro-inflammatory genes in the skin of the *APOE*$^{-/-}$ mice regarding mast cells activation markers (*TPS1, TSP2*), pro-inflammatory cytokines (*IFNG, TNFA*), and macrophage marker (*CD68*) (data not shown).

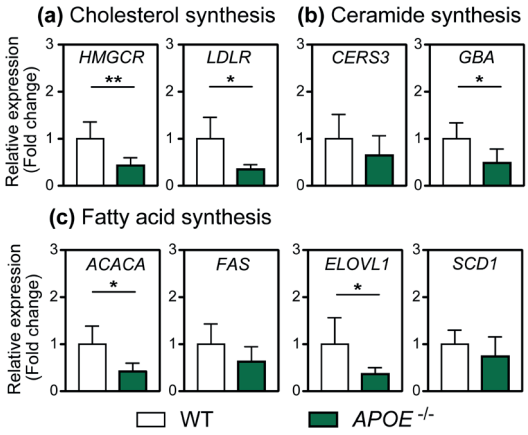

Figure 3. Downregulated mRNA expression of cholesterol, CER and FFA synthesis genes in the skin of hypercholesterolemic *APOE*$^{-/-}$ mice. The expression of genes encoding for key proteins and enzymes involved in (a) cholesterol, (b) ceramide and (c) fatty acid synthesis were measured: HMG-CoA reductase (*HMGCR*), LDL receptor (*LDLR*), ceramide synthase 3 (*CERS3*), glucocerebrosidase (*GBA*), acetyl-Coenzyme A carboxylase alpha (*ACACA*), fatty acid synthase (*FAS*), elongation of very long chain 1 (*ELOVL1*), stearoyl-Coenzyme A desaturase 1 (*SCD1*) (*p<0.05, ** p <0.01).

3.4 Lipids in the epidermis of *APOE*$^{-/-}$ mice adopt orthorhombic lateral packing

Changes in the epidermal lipid composition can alter the lateral organization of these lipids and, consequently, the integrity of the skin barrier. Therefore, the lateral organization of barrier lipids was determined by Fourier transform infrared spectrometry (FTIR). In all samples, at low temperatures the lipids had a low conformational disorder represented by frequencies below 2850 cm^{-1} for the CH_2 symmetric stretching vibrations and slightly increased with higher temperatures (Fig. 4a). From 38°C onwards this gradual shift was more pronounced indicating the transition of the lipids towards the fluid phase (frequencies above 2852 cm^{-1}). Throughout this transition the lipids in the *APOE*$^{-/-}$ epidermis showed slightly higher vibration frequencies than that of the lipids in epidermis of WT mice. The CH_2 rocking vibrations at 32°C (skin temperature) showed an orthorhombic lateral packing in a fraction of the lipids represented by the presence of a doublet: a strong peak at 719 cm^{-1} and a weaker peak at 730 cm^{-1} (Fig. 4b). The fraction of lipids in an orthorhombic packing is comparable between groups as the area ratio of the two peaks was similar for all samples (Fig. 4c). Transition temperature from orthorhombic to hexagonal phases was determined by the disappearance of the peak at 730 cm^{-1} and it was not different between groups, varying from 40-44°C (Supplementary Fig. S4).

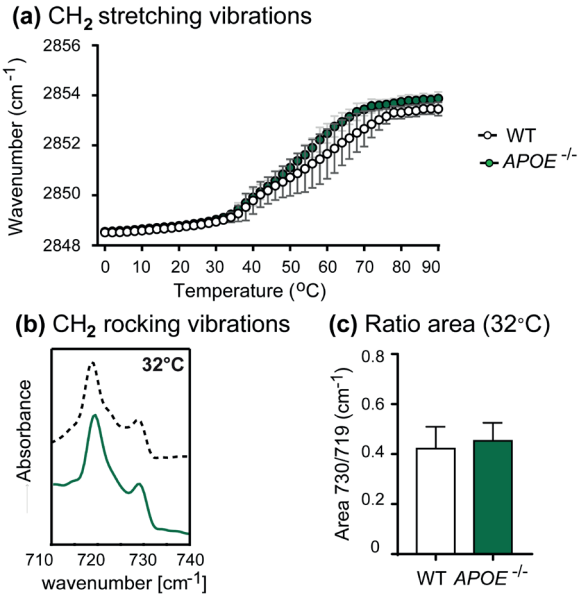

Figure 4. Altered epidermis FFA composition does not modify the orthorhombic lateral lipid organization in the skin *APOE*$^{-/-}$ mice. FTIR was used to determine the lateral packing of lipids in the epidermis of WT and *APOE*$^{-/-}$ mice. (a) CH_2 symmetric stretching vibrations (2848-2856 cm^{-1}) were plotted

against temperature (0-90°C) to follow the phase transition of the lipids; (b) CH_2 rocking vibrations (710-740 cm^{-1}) plotted at skin temperature (32°C); (c) ratio between peak area at 730 cm^{-1} and peak area at 719 cm^{-1} (32°C).

3.5 Altered FFA profile in the *APOE*$^{-/-}$ epidermis increases TEWL *in vivo* and the permeability in murine lipid model membranes (mLMM)

To examine whether the changes in FFA composition observed in the *APOE*$^{-/-}$ epidermis impairs skin barrier function, the TEWL (water loss from the skin) of WT and *APOE*$^{-/-}$ mice was measured. The TEWL of *APOE*$^{-/-}$ mice was significantly higher (12.9±0.5 g/m^2h) than that observed for the WT control (10.9±0.6 g/m^2h) (p<0.01). To further study whether the lipid barrier and in particular the change in FFA composition contributed to the impaired skin barrier function, permeation studies were performed using mLMMs. The mLMMs had a fixed CER composition, but a FFA composition mimicking that in the WT epidermis (WT_{LMM}) or in the *APOE*$^{-/-}$epidermis (*APOE*$^{-/-}{}_{LMM}$). The lamellar and lateral lipid organizations of the mLMMs were characterized by small- and wide-angle X-ray diffraction studies. The lipids in both WT_{LMM} and *APOE*$^{-/-}{}_{LMM}$ assembled in a long and short periodicity phases with no differences in the repeated distances (Fig. 5b). In the *APOE*$^{-/-}{}_{LMM}$ fewer lipids adopted an orthorhombic lateral packing compared to the WT_{LMM} as seen by the lower peak with 0.378 nm spacing in the wide-angle X-ray diffraction (Fig. 5c).

To assess the functionality of the barrier ethyl para-aminobenzoic acid (E-PABA), a commonly used topical anesthetic, was chosen as model drug for the permeability studies. A steady state flux of E-PABA was achieved in approximately 3 hours for both types of mLMM (Fig. 5d) with significantly increased flux through the *APOE*$^{-/-}{}_{LMM}$ in comparison to the WT_{LMM} (40±3.3 v.s. 14±2.2 μg/cm^2/h) (Fig. 5e). After diffusion, analysis of the donor and the collected acceptor solution showed nearly 100% drug recovery in both groups (data not shown).

4. DISCUSSION

In this study we showed for the first time that severe systemic hypercholesterolemia associated with apoE deficiency in young adult mice affects the lipid composition and barrier function of the epidermis, while in LDLR deficiency with mild hypercholesterolemia the epidermis was not affected. Here, we focused on chow diet fed and young adult mice to specifically investigate the effects of mild and severe hypercholesterolemia on barrier lipid composition and function.

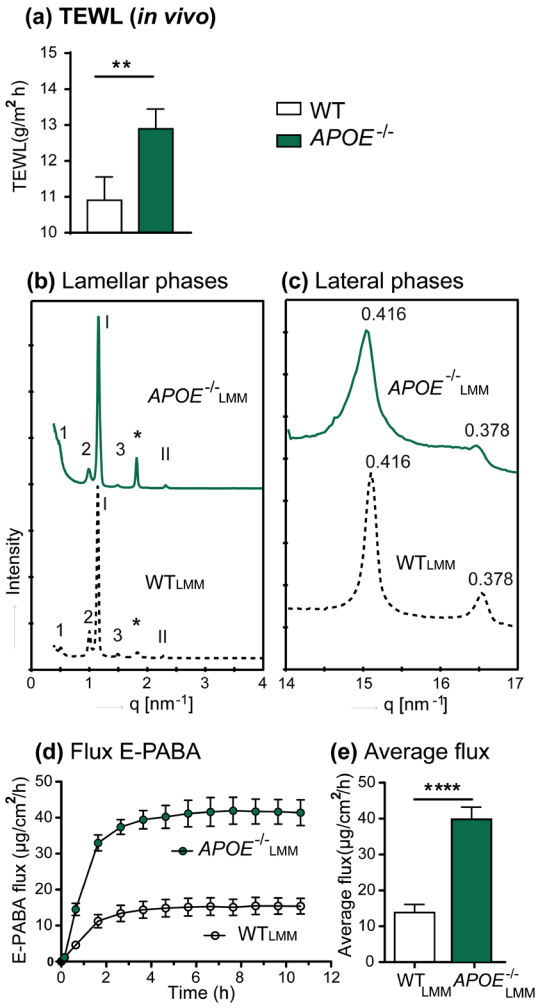

Figure 5. Skin of *APOE*$^{-/-}$ mice shows higher transepidermal water loss (TEWL) than WT control *in vivo* and epidermal lipid composition of *APOE*$^{-/-}_{LMM}$ mice shows remarkable increase in lipid barrier permeability to ethyl para-aminobenzoic acid (E-PABA). (a) Average TEWL at the skin surface of WT and *APOE*$^{-/-}$ mice. Data was collected for 90 s in vivo using a close-chamber evaporimeter. (b) Lamellar and (c) lateral organizations of murine lipid model membranes (mLMM) representing the epidermal lipids of the WT and *APOE*$^{-/-}$ mice determined by small angle- and wide angle X-ray diffraction, respectively. In Arabic numbers (1-3) the long periodicity phase orders, in Roman numbers (I-II) the short periodicity phase orders. Asterisk indicates the reflection of crystalline cholesterol. Flux of E-PABA through WT_{LMM} (open circles) and *APOE*$^{-/-}_{LMM}$ (closed circles) (d) over time (10.5 hours) and (e) at steady state (average). Data represents three different experiments (n=6-7/group) (**p<0.01; ****p<0.0001).

Analysis of the epidermal lipid composition showed similar levels of cholesterol in the *APOE*$^{-/-}$ epidermis compared to the WT controls despite the significant increase in circulating cholesterol[8,9]. However, based on the q-PCR data a higher cholesterol uptake from the circulation is expected and the skin cholesterol homeostasis is likely maintained by local reduction of cholesterol synthesis (*HMGCR*) and uptake from the circulation (*LDLR*). In line, higher intake of 25-hydroxy-cholesterol by keratinocytes *in vitro* reported downregulation of *HMGS1*[25] and suppressed the de novo cholesterol synthesis in these cells[26].

The FFA composition of the epidermis of *APOE*$^{-/-}$ mice greatly differed from the composition of the control mice with higher FFA content, characterized by a shift towards shorter and unsaturated chains. FFAs and CERs share a common biosynthetic pathway in the epidermis and alterations in the FFA chain length or unsaturation translate into similar trends in the CER profile[27,28]. Conversely, in our study the remarkable changes in FFA of the *APOE*$^{-/-}$ epidermis were not associated with alterations in the CER unsaturation and chain length profiles. This suggests that the observed changes in the FFAs may not be related to local biosynthesis, which is supported by the reduced expression of genes involved in FFA synthesis and elongation (*ACACA* and *ELOVL1*) in the *APOE*$^{-/-}$ epidermis. ELOVL1 is the main enzyme responsible for elongation of FA C20-C24 with especially high activity towards saturated and unsaturated FA C20-C22[29]. ELOVL1 activity can be inhibited *in vitro* by FA C18:1 in a dose-dependent manner[30]. Similar to the epidermis of *APOE*$^{-/-}$mice, in *ELOVL1*$^{-/-}$ mice the abundance of FFA and CER containing FA ≥C26 was strongly reduced with lower elongation activity towards FA C20-C22-CoA[27]. Interestingly, in this study no changes were observed in mRNA levels of *SCD1,* encoding for the rate-limiting enzyme in the desaturation of FFA[31]. However, SCD1 expression is strictly regulated in both gene and protein levels, usually showing a fast turn off; thus, further differences should be evaluated in protein and enzyme activity levels[32,33].

Altogether, our LC/MS and q-PCR data suggests an increased flux of cholesterol and FFA from the plasma into the skin. In the plasma, cholesterol is mainly transported as CE in the core of lipoproteins. After cellular uptake, the CE-rich core of the lipoprotein remnants is metabolized into free cholesterol and FA. In mice, plasma CE is mostly formed by esterification of cholesterol with unsaturated FA and LC/MS/MS analysis of hypercholesterolemic *APOE*$^{-/-}$ plasma shows more than 2-fold higher levels of FA C18:1-derived CE compared to the normolipidemic WT mice[7]. Similar to the plasma, we found increased amounts of FA C18:1 but also FA C18:2, an essential FA, in the epidermis of *APOE*$^{-/-}$ mice. Interestingly, the incubation of HaCaT keratinocytes with FA C18:1 increased the mRNA levels of *HMGCS1* and the activity of HMGCoA synthase promoter.

However, combined incubation of these cells with FA C18:1 and 25-hydroxy cholesterol resulted in downregulation of sterol synthesis[25]. Thus, it is possible that a higher uptake of CE-rich lipoproteins by keratinocytes of *APOE*$^{-/-}$ mice leads (1) to activation of compensatory feedback regulation in local lipid synthesis, at least on mRNA level, and (2) to the incorporation of FFAs derived from the CE-rich particles into the SC lipid matrix.

Modifications of skin lipid content and morphology have been previously described using other hyperlipidemic mouse models[8–10,34]. These modifications were mostly analyzed in double-knockout mice on *LDLR*$^{-/-}$ or *APOE*$^{-/-}$ backgrounds; in which two opposite effects occur: (1) hyperlipidemia by impaired (V)LDL pathway and (2) hypolipidemia by impaired high-density lipoprotein pathway. In these studies, double-knockout mice generated on *LDLR*$^{-/-}$ background (mild hyperlipidemic model) developed skin free cholesterol and CE accumulation, and inflammation in association with high cholesterol/high fat diets but not on chow diet. In contrast, the double-knockout with *APOE*$^{-/-}$ background (severe hyperlipidemic model) developed these alterations spontaneously in time. Thus, in line with our results this indicates that the severity of the hypercholesterolemia of the genetic background plays an important role in the development of the skin phenotypes.

Nonetheless, it is important to note that apoE and the LDLR are expressed in murine skin[18,35–37]. The role of apoE in the skin remains to be elucidated, but the role of LDLR as a mediator for the uptake of lipoproteins by the skin has been described[35]. Thus, the absence of these proteins/receptors in the skin of our mouse models may contribute to the changes reported in this study. Although CE levels are elevated in the plasma of *LDLR*$^{-/-}$ mice as compared to WT controls, the epidermal lipid profile is not affected in the skin of these mice. In this line, it could be hypothesized that LDLR deficiency in the skin of these mice prevented the accumulation of the CE-derived lipids. Additionally, considering the hypercholesterolemia as the driving factor altering the composition of the epidermal lipids, *LDLR*$^{-/-}$ mice on chow diet develop only a minor hypercholesterolemic phenotype[11], which in turn could have led to lower skin lipoprotein accumulation. In this view, skin-specific deletion of lipid transporters (*e.g.* LDLR, CD36) on a WT and on an *APOE*$^{-/-}$ background may help elucidate the mechanisms underlying this plasma-skin lipid crosstalk.

Studies using lipid model membranes or diseased skin reported that elevated FFA content increases the fraction of lipids assembled in an orthorhombic packing[28,38.] In contrast, shorter chain lengths and/or higher degree of unsaturation of FFA species also in the presence of the same CER composition favors a hexagonal packing and

higher permeability of the lipid barrier[24,39]. As all these changes are present in the *APOE*$^{-/-}$ epidermis, these opposite effects may counteract maintaining the dense lipid orthorhombic organization. However, when interpreting FTIR results one must remember that not only cholesterol, CERs and FFAs are present on the skin surface; and these vibrations are influenced by other lipid species; e.g. sebum lipids, which are abundantly present in mouse skin[40–42].

Direct *ex vivo* analysis of SC barrier function in non-nude mice is limited by the high density of hair follicles, which hinders the isolation of the few SC layers or the intact viable epidermis. Additionally, the high number of hair follicles offers an additional route of permeation for model drugs when studying skin barrier integrity[43,44]. TEWL is a well-established method to monitor the water loss from the skin and to assess the functionality of the SC barrier[45,46]. A decrease in TEWL values has been strongly correlated with a reduced chain length of the FFAs and CERs in the SC, emphasizing the importance of SC lipids for the skin barrier function[28]. Similarly, the skin of *APOE*$^{-/-}$ mice showed a reduced SC barrier function characterized by higher TEWL and a change in the fatty acid composition.

Additionally, mLMMs were used as *APOE*$^{-/-}$ SC substitutes to assess the contribution of the *APOE*$^{-/-}$ epidermal lipid composition to the impairment of the skin barrier function. Higher degree of unsaturation of the FFAs correlates with a lower the fraction of lipids forming an orthorhombic packing in the SC or lipid model membranes[24,28], while an increased abundance of short chain FFAs may, already at low levels, show higher mobility in lipid model membranes associated with a great increase in the permeability of the lipid model membrane to E-PABA[47]. In agreement, the altered FFA composition of *APOE*$^{-/-}$ epidermis resulted in higher permeability to E-PABA through $APOE^{-/-}_{LMM}$ compared to WT_{LMM}. Our mLMMs comprised 5% of FFA C16-C18 as we aimed to study the differences in permeability associated with epidermal barriers lipids. Higher levels of these short chain FFAs would only further increase the permeability of the $APOE^{-/-}_{LMM}$, especially considering that unsaturated FFA C16-C18 are higher in the *APOE*$^{-/-}$ epidermis.

In conclusion, we show that the hypercholesterolemia in young adult *APOE*$^{-/-}$ mice affects the skin lipid composition and is associated with a compromised lipid barrier function. Our data suggests that the severity of the hypercholesterolemia and plasma CE levels may play critical roles in the development of this skin phenotype. This highlights the relevance of investigating the composition and functionality of the skin barrier of hypercholesterolemic patients at young age and prior the development of inflammatory processes as to our knowledge this information is not yet available. In turn, it may be possible to protect the skin of these patients and prevent future development of skin

inflammatory phenotypes.

CONFLICT OF INTEREST

The authors have no conflict of interest.

ACKNOWLEDGEMENTS

We thank the company Evonik (Essen, Germany) for providing the synthetic ceramides; the DUBBLE beam line team for assissting with the X-ray diffraction studies at the European Synchrotron Radiation Facility (Grenoble, France). We thank Richard W. J. Helder, Dr. Ilze Bot and Prof. Johan Kuiper for supporting the TEWL studies. This research was supported by the Leiden Academic Centre for Drug Research (Leiden University, Leiden, The Netherlands).

REFERENCES

1. Harada-Shiba, M. et al. Guidelines for Diagnosis and Treatment of Familial Hypercholesterolemia 2017. J. Atheroscler. Thromb. 751–770 (2018). doi:10.5551/jat.CR003

2. Awan, Z. et al. APOE p.Leu167del mutation in familial hypercholesterolemia. Atherosclerosis 231, 218–222 (2013).

3. Holven, K. B. et al. Subjects with familial hypercholesterolemia are characterized by an inflammatory phenotype despite long-term intensive cholesterol lowering treatment. Atherosclerosis 233, 561–567 (2014).

4. Ohshiro, T., Shimabukuro, T., Sunagawa, M. & Ohta, T. An 11-year-old boy with familial hypercholesterolemia showing multiple xanthomas and advanced atherosclerosis, who responded to lipid-lowering therapy using statin. J. Atheroscler. Thromb. 16, 698–701 (2009).

5. Aljenedil, S., Ruel, I., Watters, K. & Genest, J. Severe xanthomatosis in heterozygous familial hypercholesterolemia. J. Clin. Lipidol. 12, 872–877 (2018).

6. Getz, G. S. & Reardon, C. A. Do the Apoe −/− and Ldlr −/− Mice Yield the Same Insight on Atherogenesis? Arterioscler. Thromb. Vasc. Biol. 36, 1734–1741 (2016).

7. Subbaiah, P. V. et al. Regulation of plasma cholesterol esterification by sphingomyelin: Effect of physiological variations of plasma sphingomyelin on lecithin-cholesterol acyltransferase activity. Biochim. Biophys. Acta - Mol. Cell Biol. Lipids 1821, 908–913 (2012).

8. Accad, M. et al. Massive xanthomatosis and altered composition of atherosclerotic lesions in hyperlipidemic mice lacking acyl CoA:cholesterol acyltransferase 1. J. Clin. Invest. 105, 711–719 (2000).

9. Arnaboldi, F. et al. High-density lipoprotein deficiency in genetically modified mice deeply affects skin morphology: A structural and ultrastructural study. Exp. Cell Res. 338, 105–112 (2015).

10. Zabalawi, M. et al. Inflammation and skin cholesterol in LDLr −/− , apoA-I −/− mice: link between cholesterol homeostasis and self-tolerance? J. Lipid Res. 48, 52–65 (2007).

11. Ishibashi, S., Goldstein, J. L., Brown, M. S., Herz, J. & Burns, D. K. Massive Xanthomatosis and Atherosclerosis in cholesterol-fed low density lipoprotein receptor-negative mice. J. Clin. Invest. 93, 1885–1893 (1994).

12. Feingold, K. R. et al. Apolipoprotein E Deficiency Leads to Cutaneous Foam Cell Formation in Mice. J. Invest. Dermatol. 104, 246–250 (1995).

13. Ang, L. S., Cruz, R. P., Hendel, A. & Granville, D. J. Apolipoprotein E, an important player in longevity and age-related diseases. Exp. Gerontol. 43, 615–622 (2008).

14. Hiebert, P. R. et al. Granzyme B contributes to extracellular matrix remodeling and skin aging in apolipoprotein E knockout mice. Exp. Gerontol. 46, 489–499 (2011).

15. Elias, P. M. Stratum corneum defensive functions: An integrated view. J. Invest. Dermatol. 125, 183–200 (2005).

16. Ponec, M., Weerheim, A., Lankhorst, P. & Wertz, P. New acylceramide in native and reconstructed epidermis. J. Invest. Dermatol. 120, 581–588 (2003).

17. Lin, M.-H. & Khnykin, D. Fatty acid transporters in skin development, function and disease. Biochim. Biophys. Acta 1841, 362–8 (2014).

18. Mommaas, M., Tada, J. & Ponec, M. Distribution of low-density lipoprotein receptors and apolipoprotein B on normal and on reconstructed human epidermis. J. Dermatol. Sci. 2, 97–105 (1991).

19. Tsuruoka, H. et al. Scavenger receptor class B type I is expressed in cultured keratinocytes and epidermis. Regulation in response to changes in cholesterol homeostasis and barrier requirements. J. Biol. Chem. 277, 2916–2922 (2002).

20. Out, R. et al. Macrophage ABCG1 Deletion Disrupts Lipid Homeostasis in Alveolar Macrophages and Moderately Influences Atherosclerotic Lesion Development in LDL Receptor-Deficient Mice. Arterioscler. Thromb. Vasc. Biol. 26, 2295–2300 (2006).

21. Boiten, W., Absalah, S., Vreeken, R., Bouwstra, J. & van Smeden, J. Quantitative analysis of ceramides using a novel lipidomics approach with three dimensional response modelling. Biochim. Biophys. Acta - Mol. Cell Biol. Lipids 1861, 1652–1661 (2016).

22. Motta, S. et al. Ceramide composition of the psoriatic scale. BBA - Mol. Basis Dis. 1182, 147–151 (1993).

23. Chomczynski, P. & Sacchi, N. The single-step method of RNA isolation by acid guanidinium thiocyanate–phenol–chloroform extraction: twenty-something years on. Nat. Protoc. 1, 581–585 (2006).

24. Mojumdar, E. H., Helder, R. W. J., Gooris, G. S. & Bouwstra, J. A. Monounsaturated fatty acids reduce the barrier of stratum corneum lipid membranes by enhancing the formation of a hexagonal lateral packing. Langmuir 30, 6534–6543 (2014).

25. Siefken, W., Höppner, H. & Harris, I. R. Regulation of cholesterol synthesis by oleic and palmitic acid in keratinocytes. Exp. Dermatol. 9, 138–145 (2000).

26. Ponec, M., Havekes, L., Kempenaar, J. & Jan Vermeer, B. Cultured Human Skin Fibroblasts and Keratinocytes: Differences in the Regulation of Cholesterol Synthesis. J. Invest. Dermatol. 81, 125–130 (1983).

27. Sassa, T. et al. Impaired Epidermal Permeability Barrier in Mice Lacking Elovl1, the Gene Responsible for Very-Long-Chain Fatty Acid Production. Mol. Cell. Biol. 33, 2787–2796 (2013).

28. van Smeden, J. et al. The importance of free fatty acid chain length for the skin barrier function in atopic eczema patients. Exp. Dermatol. 23, 45–52 (2014).

29. Ohno, Y. et al. ELOVL1 production of C24 acyl-CoAs is linked to C24 sphingolipid synthesis. Proc. Natl. Acad. Sci. 107, 18439–18444 (2010).

30. Sassa, T., Wakashima, T., Ohno, Y. & Kihara, A. Lorenzo's oil inhibits ELOVL1 and lowers the level of sphingomyelin with a saturated very long-chain fatty acid. J. Lipid Res. 55, 524–530 (2014).

31. Kim, H.-J., Miyazaki, M. & Ntambi, J. M. Dietary cholesterol opposes PUFA-mediated repression of the stearoyl-CoA desaturase-1 gene by SREBP-1 independent mechanism. J. Lipid Res. 43, 1750–1757 (2002).

32. Mauvoisin, D. & Mounier, C. Hormonal and nutritional regulation of SCD1 gene expression. Biochimie 93, 78–86 (2011).

33. Sampath, H. & Ntambi, J. M. Role of stearoyl-CoA desaturase-1 in skin integrity and whole body energy balance. J. Biol. Chem. 289, 2482–2488 (2014).

34. Aiello, R. J. et al. Increased atherosclerosis in hyperlipidemic mice with inactivation of ABCA1 in macrophages. Arterioscler. Thromb. Vasc. Biol. 22, 630–637 (2002).

35. Abd El-Latif, M. I. A., Murota, H., Terao, M. & Katayama, I. Effects of a 3-hydroxy-3-methylglutaryl coenzyme A reductase inhibitor and low-density lipoprotein on proliferation and migration of keratinocytes. Br. J. Dermatol. 128–137 (2010).

36. Gordon, D. A., Fenjves, E. S., Williams, D. L. & Taichman, L. B. Synthesis and secretion of apolipoprotein E by cultured human keratinocytes. J.Invest Dermatol. 92, 96–99 (1989)

37. Newman, T. C., Dawson, P. A., Rudel, L. L. & Williams, D. L. Quantitation of apolipoprotein E mRNA in the liver and peripheral tissues of nonhuman primates. J. Biol. Chem. 260, 2452–2457 (1985).

38. Groen, D., Poole, D. S., Gooris, G. S. & Bouwstra, J. A. Investigating the barrier function of skin lipid models with varying compositions. Eur. J. Pharm. Biopharm. 79, 334–342 (2011).

39. Groen, D., Poole, D. S., Gooris, G. S. & Bouwstra, J. A. Is an orthorhombic lateral packing and a proper lamellar organization important for the skin barrier function? Biochim. Biophys. Acta - Biomembr. 1808, 1529–1537 (2011).

40. Ludovici, M. et al. Influence of the sebaceous gland density on the stratum corneum lipidome. Sci. Rep. 8, 1–12 (2018).

41. Smith, K. R. & Thiboutot, D. M. Thematic review series: Skin Lipids. Sebaceous gland lipids: friend or foe? J. Lipid Res. 49, 271–281 (2008).

42. Westerberg, R. et al. Role for ELOVL3 and Fatty Acid Chain Length in Development of Hair and Skin Function. J. Biol. Chem. 279, 5621–5629 (2004).

43. Blume-Peytavi, U. et al. Follicular and percutaneous penetration pathways of topically applied minoxidil foam. Eur. J. Pharm. Biopharm. 76, 450–453 (2010).

44. Mohd, F., Todo, H., Yoshimoto, M., Yusuf, E. & Sugibayashi, K. Contribution of the hair follicular pathway to total skin permeation of topically applied and exposed chemicals. Pharmaceutics 8, (2016).

45. Nomoto, K. et al. Epidermal permeability barrier function and sphingolipid content in the skin of sphingomyelin synthase 2 deficient mice. Exp. Dermatol. 27, 827–832 (2018).

46. Fluhr, J. W., Feingold, K. R. & Elias, P. M. Transepidermal water loss reflects permeability barrier status : validation in human and rodent in vivo and ex vivo models. Exp. Dermatol. 15, 483–492 (2006).

47. Uchiyama, M., Oguri, M., Mojumdar, E. H., Gooris, G. S. & Bouwstra, J. A. Free fatty acids chain length distribution affects the permeability of skin lipid model membranes. Biochim. Biophys. Acta - Biomembr. 1858, 2050–2059 (2016).

SUPPLEMENTARY INFORMATION

1. MATERIALS AND METHODS

1.1 Chemicals

Ketamine and atropine were purchased from AUV Veterinary Services (Cuijk, The Netherlands); xylazine from ASTFarma (Oudewater, The Netherlands); Kaiser's glycerol gelatin and sodium chloride (NaCl) from Boom (Meppel, The Netherlands). Sodium phosphate dibasic (Na_2HPO_4), hematoxylin, eosin, toluidine blue, trypsin from bovine pancreas, trypsin inhibitor, cholesterol, free fatty acids (FFA) C16-C30, deuterated FFA C18 and deuterated FFA C24, chloroform, acetic acid, deuterated water (D_2O), sodium bromide (NaBr), ethyl-para-aminobenzoic acid (E-PABA), trifluoroacetic acid were purchased from Sigma-Aldrich (Zwijndrecht, The Netherlands). Potassium dihydrogen phosphate (KH_2PO_4), potassium chloride (KCl), and Entellan® were purchased from Merck (Darmstadt, Germany). CER[NS] (C24deuterated; C18protonated) and all synthetic CER were kindly provided by Evonik Industries (Essen, Germany). Heptane was purchased from ChemLab (Zedelgem, Belgium). Methanol, ethanol, isopropanol and acetonitrile were purchased from Biosolve (Valkenswaard, The Netherlands). All solvents used were analytical grade.

1.2 Liquid chromatography-mass spectrometry (LC/MS)

Table S1. Gradient of solvents used for cholesterol and CER analysis by UPLC-LC/MS.

Run time (min)	Solvent A[1] (%)	Solvent B[2] (%)
0	98	2
2.5	96	4
2.6	93	7
6	88	12
11	50	50
13	98	2

[1]**Solvent A - 100% Heptane**

[2]**Solvent B -Heptane:isopropanol:ethanol - 50:25:25; v/v/v**

Table S2. Gradient of the solvents used for FFA analysis by UPLC-LC/MS.

Run time (min)	Solvent A[1] (%)	Solvent B[2] (%)
0	100	0
2.5	0	100
5	0	100
8	100	0
11	100	0

[1]Solvent A - Acetonitrile/milliQ/chloroform/acetic acid -90:10:2:0.005; v/v/v/v

[2]Solvent B -Methanol/heptane/chloroform/acetic acid -90:10:2:0.005; v/v/v/v

1.3. Quantitative real-time PCR (q-PCR)

Table S3. Forward and reverse primer sequences used for q-PCR.

Protein (Gene)	Forward primer Reverse primer
Ribosomal protein, large, P0 (RPL0)	CTGAGTACACCTTCCCACTTACTGA CGACTCTTCCTTTGCTTCAGCTTT
Cytochrome c-1 (CYC1)	ACTGGGGTGTCATTGCGAGAAGGC GGTCATGCTCTGGTTCTGATGCCCA
Ribosomal protein S20 (RPS20)	GGACTTGATCAGAGGCGCCAAGGAAA CCCAGGTCTTGGAACCTTCACCACAA
Acetyl-Coenzyme A carboxylase alpha (ACACA)	GGAAGATGGCGTCCGCTCTGTG GTGAGATGTGCTGGGTCATGTGGAC
ATP-binding cassette, subfamily A, member 1 (ABCA1)	AGAGCAAAAAGCGACTCCACATAGAA CGGCCACATCCACAACTGTCT
ATP-binding cassette, subfamily A, member 12 (ABCA12)	TGACCTTCTGGAAACCAACAAGACTGC CACTTATGGTGGAACCTTGGCTACTGG
ATP-binding cassette, subfamily G, member 1 (ABCG1)	TTGACACCATCCCAGCCTAC CAGTGCAGGTCTTCTCGGT
Aldehyde dehydrogenase family 3, subfamily A2 (ALDH3A2)	CGGGTGATAGATGAGACCTCCAGTGG AGGGGCGCTGATGAGAAAAGGTATCA
N-acylsphingosine amidohydrolase 1 (ASAH1)	TTATTGATGACCGCAGAACACCGGC TACAAGGGTCTGGGCAATCTCGAAGG
Cluster of differentiation 36 (CD36)	ATGGTAGAGATGGCCTTACTTGGG AGATGTAGCCAGTGTATATGTAGGCTC
Cluster of differentiation 68 (CD68)	TGCCTGACAAGGGACACTTCGGG GCGGGTGATGCAGAAGGCGATG

Protein (Gene)	Forward primer Reverse primer
Ceramide kinase 1 (CERK1)	CTTGCTCAGCCTCCAGAAGCTCCT TCCTGGGCTTTGGGGTTCTTGCTTA
Ceramide synthase 3 (CERS3)	GGGCCTCCACGTTTACTGGGGT GCCCTTGGTGCTCTCTGCTTCCT
Elongation of very long chain fatty acids 1 (ELOVL1)	GGCAGAACTTGCCCCTGAGAAGAA TTCACAACAGCCTCCATCCTGGC
Elongation of very long chain fatty acids 4 (ELOVL4)	TGGAATCAAGTGGGTGGCTGGAGG AGCATGGTCAGGTATCGCTTCCACC
Elongation of very long chain fatty acids 6 (ELOVL6)	GGACCTGTCAGCAAATTCTGGGCTTA GGAGTACCAGGAGTACAGGAGCACA
Elongation of very long chain fatty acids 7 (ELOVL7)	ACAGCTGTGCACGTGGTCATGTATTC ACTGGGTACTGGTAATTGCAGTCCTCC
Fatty acid binding protein 5 (FABP5)	GGACGGGAAGGAGAGCACGATAACA GCACCTTCTCATAGACCCGAGTGCA
Fatty acid synthase (FAS)	GGCGGCACCTATGGCGAGG CTCCAGCAGTGTGCGGTGGTC
Fillagrin (FLG)	TTCTCAGAAGGCCAGGCAGTAGGAG CGCGTTGCTGTTCGTGCTGG
Glucocerebrosidase (GBA)	GCCCTTGCCAACAGTTCCCATGATG TGCCATGAACGTACTTAGCTGCCTCT
2-hydroxyacyl-CoA lyase 1 (HACL1)	GGTTTTGACGCTGACACCTGGGAAA CCTCAGCGAGTGTTGGAGCTCTTCT
3-hydroxy-3-methylglutaryl-CoA reductase (HMGCR)	CGAGCCACGACCTAATGAAGAATG TGCATCACTAAGGAACTTTGCACC
Interferon gamma (IFNG)	CCTTCTTCAGCAACAGCAAGGCGA GCGCTGGACCTGTGGGTTGT
Involucrin (IVL)	CCTCTGCCTTCTCCCTCCTGTGAGT ACACAGTCTTGAGAGGTCCCTGAACCA
Keratin 10 (K10)	GCGGCGACCAATCATCTAAAGGACC CCAGTGGCCCGTATGAAGAGACTCT
Antigen identified by monoclonal antibody Ki 67 (MKI67)	TCTGTGGAAGAGCAGGTTAGCACTGT TGGGCCTTGGCTGTTTTACATTGGTT
low density lipoprotein receptor (LDLR)	TGTGTGATGGAGACCGAGATTG CGTCAACACAGTCGACATCC
Stearoyl-Coenzyme A desaturase 1 (SCD1)	TACTACAAGCCCGGCCTCC CAGCAGTACCAGGGCACCA
Tumor necrosis factor alfa (TNFA)	GCCTCTTCTCATTCCTGCTTGTG ATGATCTGAGTGTGAGGGTCTGG
Tryptase alpha/beta 1 (TPS1)	ACCCTGTCCCCCTACCTCCT AATGGGAACTTGCACCTCCTTCAAA
Tryptase beta 2 (TPS2)	GCGGAGGTTCTCTCATCCATCCA CTGCTCACGAAGCTGCACCC

2. RESULTS

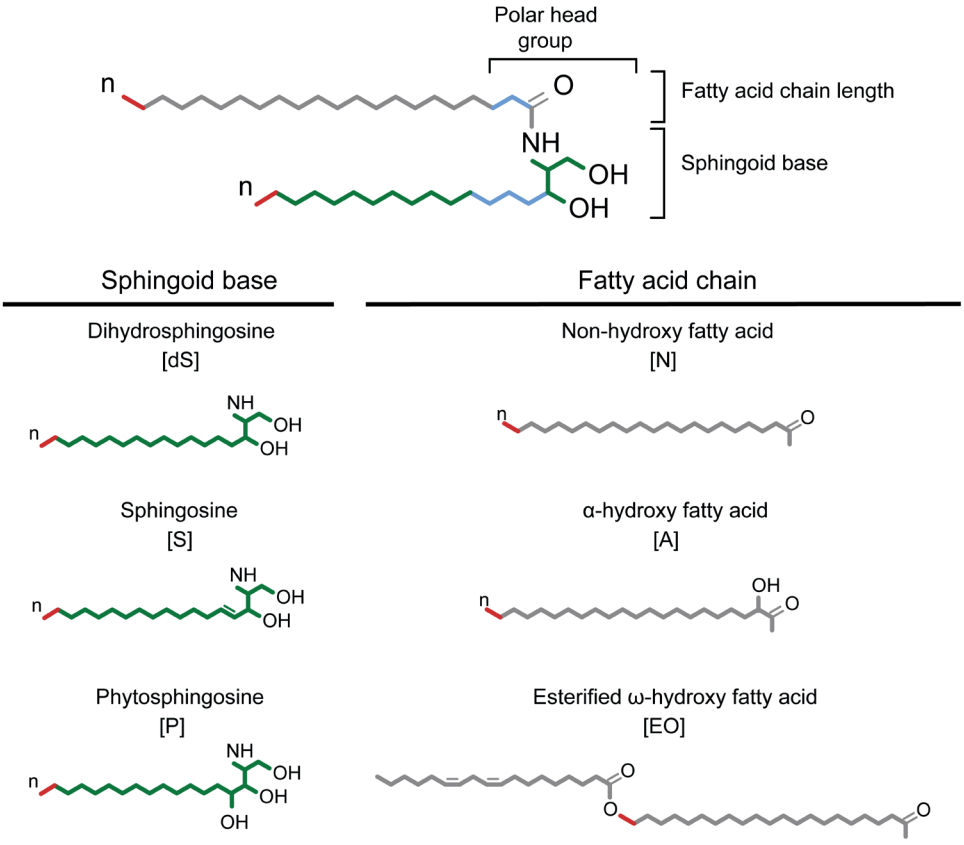

Figure S1. Schematic overview of a CER molecular structure and summary of the CER subclasses present in the epidermis of WT, *LDLR*$^{-/-}$ and *APOE*$^{-/-}$ mice. CERs consist of an acyl chain (in grey) and a sphingoid base (green), which can both vary in number of carbons (n; indicated in red). Nomenclature of ceramides subclasses (Motta *et al.* 1993)[1] based on different fatty acid acyl chains (non-hydroxy fatty acid [N]; α-hydroxy fatty acid [A]; esterified ω-hydroxy fatty acid [EO]) and on the sphingoid base (dihydrosphingosine, [dS]; sphingosine [S]; phytosphingosine [P]).

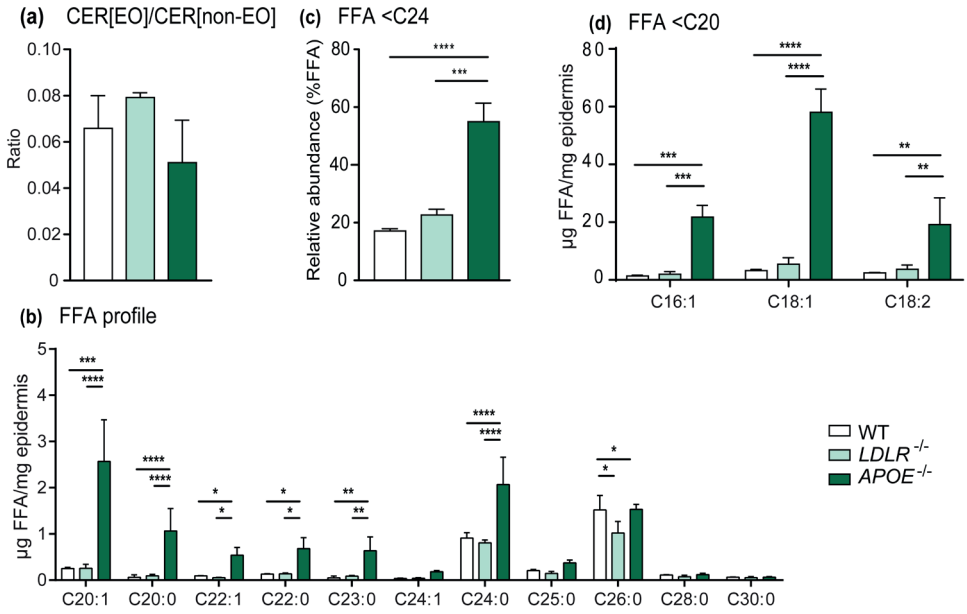

Figure S2. LC/MS analysis of WT, *LDLR*$^{-/-}$ and *APOE*$^{-/-}$ epidermal lipids. (a) Ratio CER[EO]/CER[non-EO], (b) absolute amounts FFA with chain length between C20-C30 per mg epidermis, (c) relative abundance of FFA with chain length below 24 carbon atoms, and (d)absolute amounts of FFA with chain length lower than 20 carbon atoms (n= 3 animals/group). FFA C16:0 and FFA C18:0 were not quantified due to manufacturer's contamination of the solvent with these FAs. Differences among groups were determined by One-way or Two-way ANOVAs using Holm-Šídák post-hoc test and represented as mean ± SD; *p<0.05, **p <0.01, ***p<0.001 and ***p<0.0001).

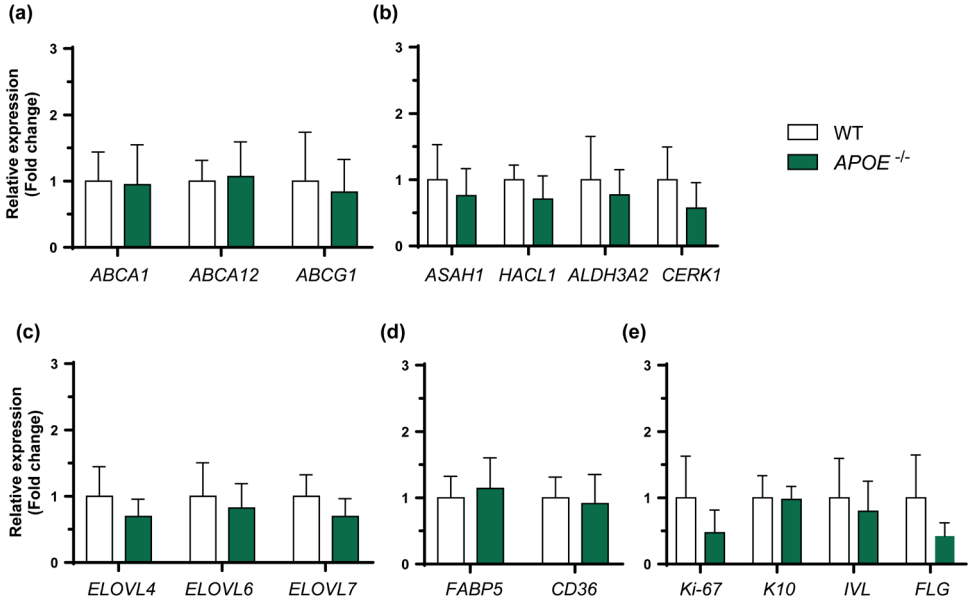

Figure S3. q-PCR of murine skin. mRNA expression of (a) ABC transporters, (b) ceramide degradation enzymes, (c) FFA elongases, (d) FFA transporters, and (e) keratinocyte proliferation and differentiation markers. Genes measured and encoded proteins: ABCA1 – ATP binding cassette class A member 1; ABCA12 – ATP binding cassette class A member 12; ABCG1 – ATP binding cassette class G member 1; ASAH1 – N-acylsphingosine amidohydrolase 1; HACL1 – 2-hydroxyacyl-CoA lyase 1; ALDH3A2 – Aldehyde dehydrogenase family 3, subfamily A2; CERK1 – Ceramide kinase 1; ELOVL4 – elongase of very long chain fatty acid 4; ELOVL6 – elongase of very long chain fatty acid 6; ELOVL7 – elongase of very long chain fatty acid 7; FABP5 – fatty acid binding protein 5; CD36 – cluster of differentiation 36; mitosis Ki-67 – Marker Of Proliferation Ki-67, K10 – early differentiation marker keratin 10, IVL – late differentiation marker involucrin; FLG – late differentiation marker filaggrin (n=6 animals/group). Statistical analysis by two-tailed unpaired students T-tests. Data presented as mean ± SD; no significant differences (p<0.05) were observed.

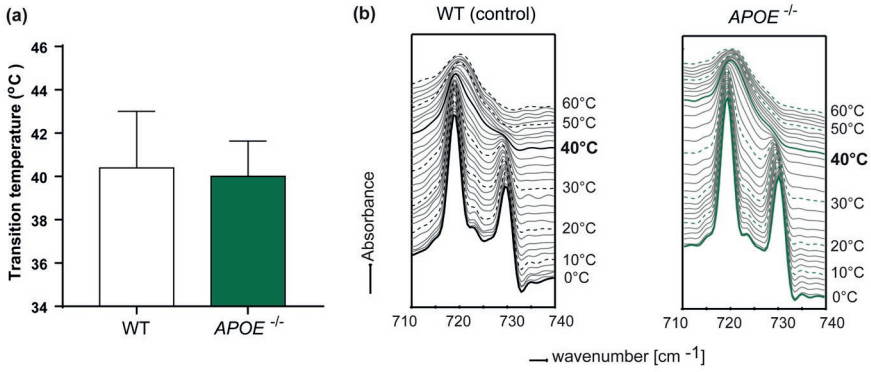

Figure S4. FTIR analysis of epidermal lipids in the skin of WT and *APOE*$^{-/-}$ mice. (a) Average transition temperature (TT) between orthorhombic and hexagonal phases determined by disappearance of the peak at 730 cm^{-1}, (b) CH_2 rocking vibrations plotted as a function of temperature (0-60°C) with TT marked in bold. (n= 4-5 animals/group). Differences between groups were determined by determined by two-tailed unpaired students T-tests. Data is presented as mean ± SD; no significant differences (p<0.05) were observed.

REFERENCES

1. Motta, S. *et al.* Ceramide composition of the psoriatic scale. BBA - Mol. Basis Dis. 1182, 147–151 (1993).